Study on the Identifiability of Material Properties Using Solely the Residual Imprint in Instrumented Indentation Experiment [†]

Mingzhi Wang and Jianjun Wu *

School of Mechanical Engineering, Northwestern Polytechnical University, Xi'an 710072, China;
wangmz_nwpu@foxmail.com

* Correspondence: wujj@nwpu.edu.cn; Tel.: +86-138-918-33046

† Presented at the 18th International Conference on Experimental Mechanics (ICEM18), Brussels, Belgium, 1–5 July 2018.

Abstract: Indentation test has been widely used to determine the mechanical properties of materials. In the present work, based on our previous developed inverse computation approach, we investigated the identifiability of the plastic properties of metal materials using solely the residual imprint in instrumented indentation. The indentation experiment was implemented on the Al 2024-t3 alloy, and result shows the experiment error exists unavoidably. To quantitatively investigate the influence of experiment error on the inverse derived material properties, the indentation simulation models were built, of which three different indenter shapes (conical, flat and spherical) and two different simulation set-ups (load or displacement control types) are considered. The sensitivity of the inverse problem in the relevant questions are systematically investigated. Results show the inverse problem formulated by the force control using a non-self-similar indenter is able to give more robust solution of the inverse derived material parameters. Besides, the numerical protocol was verified by application on the Al 2024-t3 alloy, and the plastic properties (yield stress and strain hardening exponent) obtained from indentation and uniaxial tests show good agreement.

Keywords: material properties; identifiability; indentation; residual imprint; inverse identification

1. Introduction

Indentation test has long been used as a simple and effective tool to measure the material properties, e.g., hardness [1–4]. The main advantage of this method is that, it is suitable for the specimens with finite sample volumes, where the conventional uniaxial tests are not applicable [2,3]. In order to determine the plastic properties of materials using the information collected from indentation experiment, many theories and methods have been well-established, e.g., representative stress strain method [5,6], dimensionless functions method [4,7], and the inverse finite element (FE) method [2,8]. In these previous methods [4–8], the indentation P-h curve is always considered in the indentation analysis. However, it was reported in many literatures [9–13] that, the accurate determination of indentation P-h curve is not an easy task. The following uncertainty factors can influence the accuracy of the experiment P-h curve greatly: (1) the determination of the initial zero-load and initial-displacement point [9,10]; (2) the indenter deformation and machine/frame compliance [11,12]. In order to alleviate the problems mentioned above, many researchers [2,3,13] used solely the residual imprint in the indentation analysis. It demands neither the accurate determination of indentation P-h curve, nor the specific pile-up values [2,3].

In the indentation experiment, generally three different indenter types can be considered, e.g., conical, flat punch and spherical indenters. The nature of the inverse problem, e.g., uniqueness of the inverse derived material parameters and their sensitivity to the experiment error, is very important to the practical usefulness of the established indentation methods [2,14]. So, it is very necessary to investigate the nature of the inverse problem formulated by different experiment conditions, e.g., different indenter shape and its corresponding simulation control types, when solely the residual imprint in instrumented indentation experiment is considered. In the present work, the nature of the inverse problem formulated by three different indenter shapes and two different simulation set-ups will be revealed. The reported results will be helpful for the design of indentation experiment in determining the mechanical properties of materials using solely the residual imprint in indentation experiment.
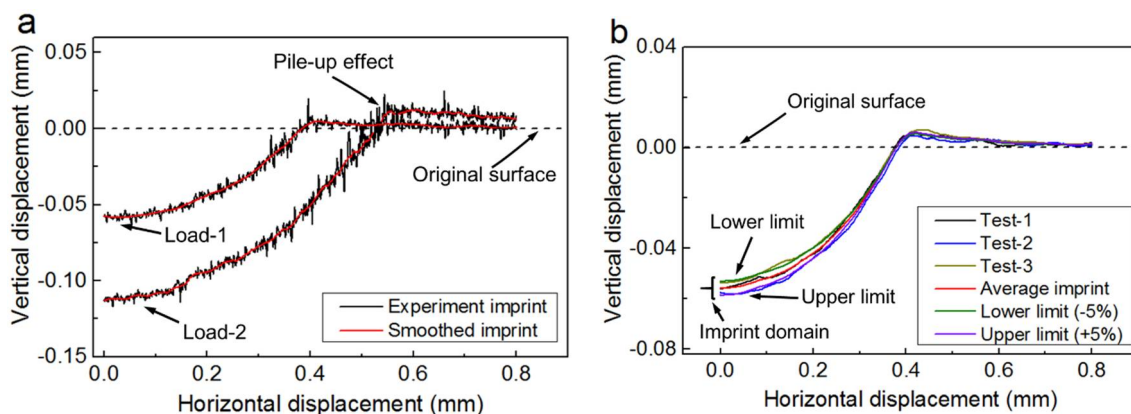
2. Experiment Investigation

The material studied here was the aluminum alloy Al 2024-t3. Uniaxial properties of this material is obtained by using tensile test that obeys the ASTM standards [15]. The plastic parameters are obtained by fitting the uniaxial stress strain curves using the Hollomon hardening model, and they are listed in Table 1.

Table 1. Uniaxial mechanical properties of Al 2024-t3.

Material	E (GPa)	σ_y (Mpa)	n
Al 2024-t3	71.50	292.3	0.137

Indentation experiment was implemented on a Hardness tester at room temperature. Indenter used in the experiment was a tungsten carbide ball, with radius 1.25 mm. The specimen was cubic, with dimensions 10 mm × 12 mm × 10 mm (length, width and height). Before indentation experiment, the surface of specimen was carefully polished into mirror finish, to avoid the influence of surface roughness. The movement of indenter was force controlled, up to a prior defined maximum load value. Holding time was 15s, and then the indenter was withdrawn gradually. The residual imprint left on the surface of specimen was measured by using the 3D Measuring Laser Microscope (OSL4000).

Figure 1. 2D residual imprints in spherical indentation experiment: (**a**) the smoothed imprint; (**b**) definition of the imprint domain.

For the each prescribed load in experiments, three repeated tests were implemented at the different indentation sites of the same specimen (denoted as Test-1, Test-2 and Test-3). Figure 1a shows the smoothed imprints obtained from Load-1: 612.745 N and Load-2: 1225.49 N. In Figure 1b, it shows that the experiment result in the three tests (Load-1: 612.745 N) of the same specimen are not unique. The experimental imprint exhibits small disturbance, as shown in Figure 1. It's noted that, the experiment error exists unavoidably, because of many uncertainty factors, e.g., material

heterogeneity and experiment imprecision [2]. Besides, the disturbance error is within $\pm 5\%$, and the experimental result obtained from several independent indentation tests forms an imprint domain, as shown in Figure 1b.

3. Identification Method

In this section, the numerical protocol developed in our previous work [2] will be used to determine the unknown plastic properties of Al 2024-t3, and further reveal the sensitivity of the inverse derived material parameters to the experiment error. Here, for the simplicity purpose, this numerical method will be briefly introduced. The vertical displacement of residual surface nodes is saved in the vector S_i, and i is the residual imprint obtained from the ith prescribed load. So, $S_i \in R^n$, and n is the number of surface nodes (it is also the dimension of vector S_i.). Liner weighting of the imprint snapshots of a material under several different indentation loads can be expressed as

$$S_{weight} = \frac{1}{M}\sum_{i=1}^{M}\lambda_i S_i \text{ and } i = 1,2,\dots,M \tag{1}$$

In Equation (1), M represents the total number of prescribed indentation loads. Vector S_{weight} is the weighted imprint snapshot of the M residual imprints. λ_i is the corresponding weighting coefficient of the ith imprint snapshot. The averaged weighting imprint $\bar{S}$ can be expressed as

$$\bar{S} = \frac{1}{N}\sum_{j=1}^{N}S_{weight}^{j} = \frac{1}{NM}\sum_{j=1}^{N}\sum_{i=1}^{M}\lambda_i S_i^{j} \tag{2}$$

where, imprint snapshots S_1^{j}, S_2^{j}, ..., S_N^{j} are obtained from the numerical simulation of N given materials c_1^*, c_2^*, ..., c_N^* at the jth prescribed indentation load. Vector $\bar{S}$ is the averaged weighting imprint. The corresponding centered weighting imprint is saved in the matrix S, and it is expressed as

$$S = [S_{weight}^1 - \bar{S}, S_{weight}^2 - \bar{S}, S_{weight}^3 - \bar{S}, \dots, S_{weight}^N - \bar{S}] \tag{3}$$

So, each snapshot S_{weight}^{i} can be reconstructed by Equation (4).

$$S_{weight}^{i} = \bar{S} + U\alpha_i = \bar{S} + \sum_{j=1}^{N}U_j\,\alpha_{ij} \tag{4}$$

In Equation (4), each U_j in U serves as the orthogonal basis of imprint snapshot S, and it is used to reconstruct the each column of matrix S. Vector α_i is the corresponding coordinate of the weighting snapshot S_{weight}^{i} in this orthogonal basis system. Therefore, the cost function can be expressed as

$$\omega(c^*) = [\alpha(c^*) - \alpha^{exp}]^T[\alpha(c^*) - \alpha^{exp}] \tag{5}$$
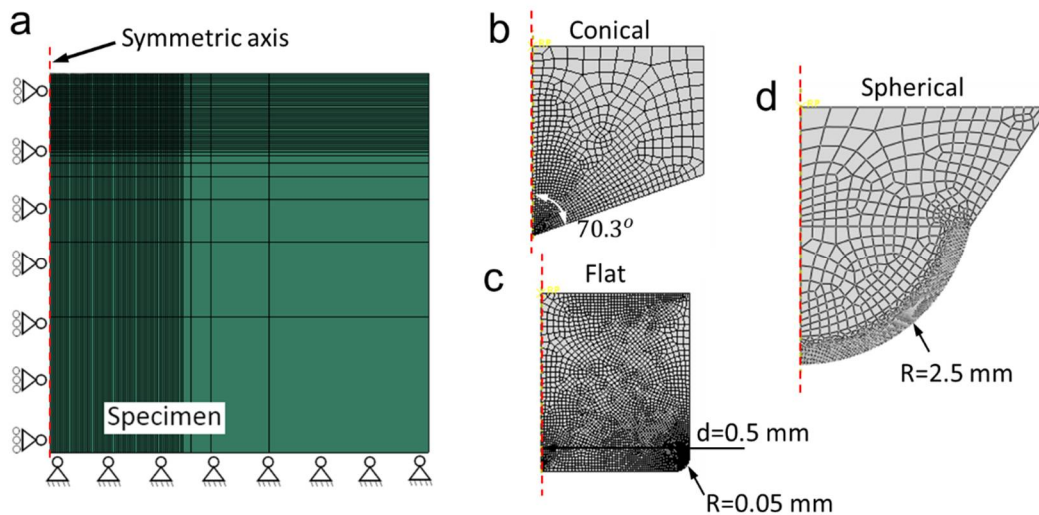
where, $\omega(c^*)$ is the error norm between experiment and simulation. $\alpha(c^*)$ is the coordinate of simulated imprint snapshot in the orthogonal basis system, while α^{exp} represents the corresponding coordinate of experiment imprint S^{exp}. Vector c^* includes the unknown material parameters that need to be determined. The inverse problem described in Equation (5) is solved by using the "Interior-point" optimization algorithm. More information about this optimization algorithm can be found in Refs [2,16]. In the present study, the iteration is convergent only when the variation of $\omega(c^*)$ is less than ε_{thr}, and ε_{thr} is defined at 1×10^{-3}.

4. Computational Modelling of Indentation Tests

The ABAQUS commercial codes [17] were used in the indentation simulations. Three different indenter shapes, conical, flat punch and spherical, are considered. Figure 2 shows the FE models and the indenters used in the indentation simulation. Because of the symmetrical properties of the indentation problem, the 2D axisymmetric boundary conditions are used. The indenter used in the simulation is deformable body, with elastic modulus 600 GPa, and Poisson's ratio 0.23 [2]. Refined meshes were created around the local contact regions between specimen and indenter.

In conical indentation simulation, the inner half angle of indenter is 70.3°. The height and radius of the selected flat indenter are 0.8 mm and 0.5 mm, respectively. A small rounding radius, 0.05 mm is used for the flat indenter, in order to avoid the stress singularity in the local contact edge. The

radius of spherical indenter is 1.25 mm. Contact friction between the surfaces of indenter and specimen was fixed at 0.1 [18]. Poisson's ratio of specimen was fixed at 0.3 [19]. Radius and height of specimen were defined at 4 mm, so that the influence of outer boundary effects is negligible. CAX4R element type was used for both the indenters and specimen. Two different control types, force control (F-C) and displacement control (D-C), are used in the present study.

Figure 2. FE model used in indentation simulation: (**a**) meshes and boundary conditions of specimen; (**b**) conical indenter; (**c**) flat indenter; (**d**) spherical indenter.

5. Results and Discussion

As we have discussed in Section 2, that the experiment result shows obvious disturbance. Here, in order to avoid the influence of the other uncertainty factors, we use the "simulated" imprint using the plastic properties, σ_y = 292.3 MPa and n = 0.137 of the target material, as the replacement of real experiment imprint. This imprint is denoted as the "original" imprint snapshot. Then, two error disturbances, −5% and +5% are added on the original imprint data. They are denoted as the upper and lower limit snapshots. These three imprint snapshots are separately used in the inverse identification process with different combinations of indenter shapes and simulation set-ups. Results are shown in Figures 3 and 4.

Because the single imprint under one certain prescribed indentation load is used here, M in Equation (1) is defined as 1, and λ_1 = 1 and λ_2 = 0. The selected material ranges in the present optimization problem are 200 MPa $\leq \sigma_y \leq$ 380 MPa, and 0.075 $\leq n \leq$ 0.195. The optimization algorithm described in Equation (5) is essentially nonlinear and non-convex. So, four different initial feasible points are selected in the inverse identification processes, in order to avoid the local minimum values. These four different initial feasible points are denoted as a: (200, 0.075), b: (200, 0.195), c: (380, 0.075) and d: (380, 0.195).
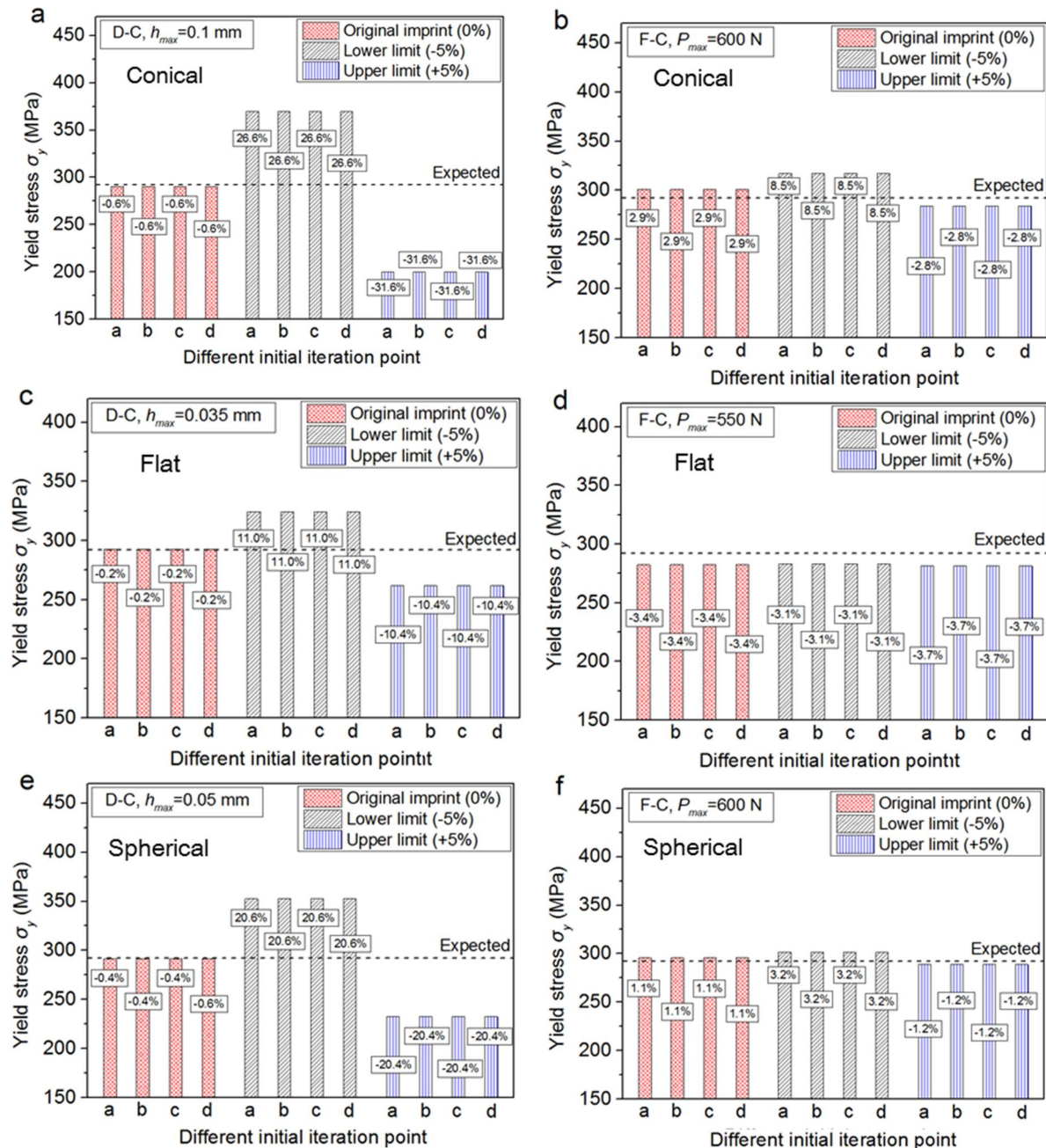
As can be seen from Figures 3 and 4, that the unique solution of the inverse derived material parameters is obtained, whatever the selected indenter shapes or simulation set-ups. The inverse identified yield stress and strain hardening exponent of the four different initial points, a–d are nearly identical. However, the stability of the inverse problem revealed by using different indenter shapes or simulation set-ups exhibits distinct difference.

First, in light of the selection of simulation set-up, it shows both the yield stress and strain hardening exponent identified by using the force-controlled simulation type are more stable, whatever the selected indenter shapes are conical, flat or spherical. When the force-control type is used, with ±5% error disturbance added on the original imprint, it only causes maximum +8.5% error of the inverse yield stress (e.g., Figure 3b using a conical indenter), and maximum −10.8% error of the inverse identified strain hardening exponent (e.g., Figure 4b using a flat indenter). In most
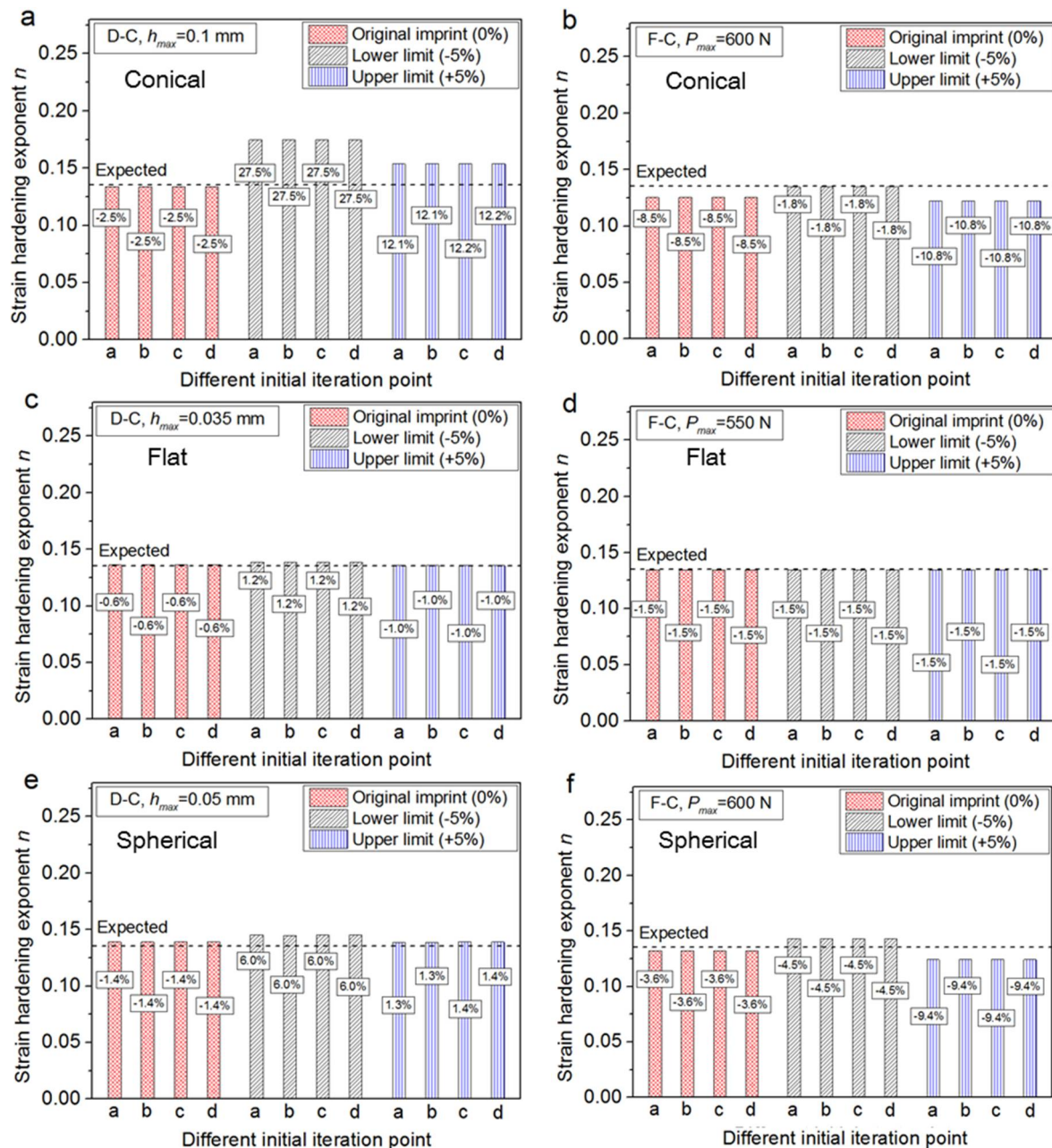
cases, the error values of the inverse identified parameters of both the yield stress and strain hardening exponent are within ±5% (e.g., Figures 3d,f and 4d,f).

Second, in light of the selection indenter types, it indicates that a non-self-similar indenter is preferred. In the displacement-control situation, it shows the parameter identified using a flat or spherical indenter is more stable than those identified using a conical indentation, as shown clearly in Figure 4c and e. This phenomenon is especially obvious when the force-controlled simulation type is used. Besides, the both the yield stress and strain hardening exponent identified using a flat indenter is better than those obtained from a spherical indenter.

Figure 3. The yield stress σ_y identified using different indenter types/simulation set-ups: in (**a,c,e**), the displacement control (D-C) type is used; in (**b,d,f**), the force control (F-C) type is used.

Figure 4. The strain hardening exponent *n* identified using different indenter types/simulation set-ups: in (**a**,**c**,**e**), the displacement control (D-C) type is used; in (**b**,**d**,**f**), the force control (F-C) type is used.

However, when the displacement control type is used, the solution of inverse identified parameters shows strong sensitivity to the experiment error. In this situation, when ±5% error disturbance are added on the original imprint, it can cause maximum −31.6% error of the inverse identified yield stress (e.g., Figure 3a using a conical indenter), and maximum +27.5% error of the inverse identified strain hardening exponent (e.g., Figure 4a using a conical indenter). In most cases, the inverse identified yield stresses shows larger than ±10% error disturbances (e.g., Figure 3a,c,e). Therefore, the displacement-controlled type is not suggested in the determination of yield stress using instrumented indentation. While, this is not the case for the identification of strain hardening exponent when the flat or spherical indenter is used. In Figure 4c,e, it shows the inverse identified strain hardening exponent is still very stable. The sensitivity results will be helpful for the design of indentation experiment in determining the plastic properties of materials using solely the residual imprint in indentation experiment.

Table 2 listed the comparison of the plastic properties of Al 2024-t3 obtained from indentation and uniaxial tests data. Here, the imprint is obtained from the spherical indenter and load-controlled experiment set-up. The maximum error of the plastic parameters are about 7.99% for the yield stress (Load-1, Test-3) and −4.16% for the strain hardening exponent (Load-2, Test-2). Result indicates the numerical approach established in our previous work [2] is very effective. Besides, using the spherical indenter and load-controlled experiment set-up is able to give stable numerical results.

Table 2. Comparison of material properties obtained from indentation and uniaxial tests data using the single imprint in spherical indentation experiment.

Al 2024-t3	σ_y (Mpa)	Error of σ_y (%)	n	Error of n (%)
Uniaxial data	292.3	-	0.137	-
Load-1: 612.745 N				
Test-1	293.43	0.387	0.1416	3.358
Test-2	270.75	−7.372	0.1377	0.511
Test-3	315.64	7.985	0.1318	−3.71
Ave.	293.27	0.331	0.1371	0.073
Std. dev.	18.3266	-	0.004029	-
Load-2: 1225.49 N				
Test-1	286.23	−2.077	0.1339	−2.263
Test-2	272.42	−6.801	0.1313	−4.161
Test-3	309.88	6.014	0.1364	−0.438
Ave.	289.51	−0.954	0.1339	−2.263
Std. dev.	15.4679	-	0.002080	-

6. Conclusions

In this paper, based on our previous established numerical method [2], we fully investigated the sensitivity of the inverse derived yield stress and strain hardening exponent of Al 2024-t3 alloys using solely the residual imprint in instrumented indentation, of which three different indenter shapes and two simulation set-ups were considered. It shows the inverse problem exhibits different extent of parameters sensitivity to the experiment error, when different combinations of indenter shapes and simulation set-ups are used. The inverse problem formulated by the force control using a non-self-similar indenter is able to give more robust solution of the inverse derived material parameters. The reported result is helpful for the design of indentation experiment, when solely the residual imprint is used to extract the mechanical properties of materials. Besides, the numerical protocol [2] was verified by its application on the Al 2024-t3 alloy, and the plastic parameters obtained from indentation and uniaxial tests show good agreement.

Author Contributions: M.W. and J.W. conceived and designed the experiments; M.W. performed the experiments; M.W. wrote the paper under the guidance of J.W.

Conflicts of Interest: The authors declare no conflict of interest.

References

1. Su, C.; Herbert, E.G.; Sohn, S.; LaManna, J.A.; Oliver, W.C.; Pharr, G.M. Measurement of power-law creep parameters by instrumented indentation methods. *J. Mech. Phys. Solids* **2013**, *61*, 517–536.
2. Wang, M.; Wu, J.; Hui, Y.; Zhang, Z.; Zhan, X.; Guo, R. Identification of elastic-plastic properties of metal materials by using the residual imprint of spherical indentation. *Mater. Sci. Eng. A* **2017**, *679*, 143–154.
3. Wu, J.; Wang, M.; Hui, Y.; Zhang, Z.; Fan, H. Identification of anisotropic plasticity properties of materials using spherical indentation imprint mapping. *Mater. Sci. Eng. A* **2018**, *723*, 269–278.
4. Dao, M.; Chollacoop, N.; Van Vliet, K.J.; Venkatesh, T.A.; Suresh, S. Computational modeling of the forward and reverse problems in instrumented sharp indentation. *Acta Mater.* **2001**, *49*, 3899–3918.

5.   Kang, S.-K.; Kim, Y.-C.; Kim, K.-H.; Kim, J.-Y.; Kwon, D. Extended expanding cavity model for measurement of flow properties using instrumented spherical indentation. *Int. J. Plast.* **2013**, *49*, 1–15.

6.   Kim, K.-H.; Kim, Y.-C.; Jeon, E.-C.; Kwon, D. Evaluation of indentation tensile properties of Ti alloys by considering plastic constraint effect. *Mater. Sci. Eng. A* **2011**, *528*, 5259–5263.

7.   Cao, Y.P.; Lu, J. A new method to extract the plastic properties of metal materials from an instrumented spherical indentation loading curve. *Acta Mater.* **2004**, *52*, 4023–4032.

8.   Bono, D.M.D.; London, T.; Baker, M.; Whiting, M.J. A robust inverse analysis method to estimate the local tensile properties of heterogeneous materials from nano-indentation data. *Int. J. Mech. Sci.* **2017**, *123*, 162–176.

9.   Brammer, P.; Bartier, O.; Hernot, X.; Mauvoisin, G.; Sablin, S.-S. An alternative to the determination of the effective zero point in instrumented indentation: Use of the slope of the indentation curve at indentation load values. *Mater. Des.* **2012**, *40*, 356–363.

10. Bouzakis, K.D.; Michailidis, N.; Hadjiyiannis, S.; Skordaris, G.; Erkens, G. The effect of specimen roughness and indenter tip geometry on the determination accuracy of thin hard coatings stress-strain laws by nanoindentation. *Mater. Charact.* **2003**, *49*, 149–156.

11. Kang, S.-K.; Kim, Y.-C.; Lee, Y.-H.; Kim, J.-Y. Determining effective radius and frame compliance in spherical nanoindentation. *Mater. Sci. Eng. A* **2012**, *538*, 58–62.

12. Kim, M.; Bang, S.; Rickhey, F.; Lee, H. Correlation of indentation load-depth curve based on elastic deformation of sharp indenter. *Mech. Mater.* **2014**, *69*, 146–158.

13. Meng, L.; Breitkopf, P.; Raghavan, B.; Mauvoisin, G.; Bartier, O.; Hernot, X. Identification of material properties using indentation test and shape manifold learning approach. *Comput. Methods Appl. Mech. Eng.* **2015**, *297*, 239–257.

14. Phadikar, J.K.; Bogetti, T.A.; Karlsson, A.M. On the uniqueness and sensitivity of indentation testing of isotropic materials. *Int. J. Solids Struct.* **2013**, *50*, 3242–3253.

15. ASTM. *ASTM E8M. Test Methods for Tension Testing of Metallic Materials (Metric)*; Annual Book of ASTM Standards; ASTM: Conshohocken, PA, USA, 2003, Volume 03.01.

16. The Math Works Inc. *User's Guide and Optimization Toolbox*, Release 3.13; The Math Works Inc.: Natick, MA, USA, 2004.

17. ABAQUS. *Analysis User's Manual v6.9*; ABAQUS Inc.: Providence, RI, USA, 2009.

18. Bowden, F.P.; Tabor, D. *The Friction and Lubrication of Solids*; Oxford University Press: Clarendon, VT, USA, 2001.

19. Bucaille, J.L.; Stauss, S.; Felder, E.; Michler, J. Determination of plastic properties of metals by instrumented indentation using different sharp indenters. *Acta Mater.* **2003**, *51*, 1663–1678.